

A Reactive Peptidic Linker for Self-Assembling Hybrid Quantum Dot–DNA Bioconjugates

Igor L. Medintz,^{*†} Lorenzo Berti,^{*,‡} Thomas Pons,^{§,§} Amy F. Grimes,^{||}
Douglas S. English,^{||} Andrea Alessandrini,[‡] Paolo Facci,[‡] and Hedi Mattossi[§]

U.S. Naval Research Laboratory, Center for Bio/Molecular Science and Engineering
Code 6900, Division of Optical Sciences Code 5611, Washington, D.C. 20375,
S3-INFM-CNR, National Research Center on nanoStructures and bioSystems at
Surfaces, Via Campi 213/A, 41100 Modena, Italy, and Department of Chemistry and
Biochemistry, University of Maryland, College Park, Maryland 20742

Received April 3, 2007; Revised Manuscript Received May 7, 2007

ABSTRACT

Self-assembly of proteins, peptides, DNA, and other biomolecules to semiconductor quantum dots (QD) is an attractive bioconjugation route that can circumvent many of the problems associated with covalent chemistry and subsequent purification. Polyhistidine sequences have been shown to facilitate self-assembly of proteins and peptides to ZnS-overcoated CdSe QDs via complexation to unoccupied coordination metal sites on the nanocrystal surface. We describe the synthesis and characterization of a thiol-reactive hexahistidine peptidic linker that can be chemically attached to thiolated-DNA oligomers and mediate their self-assembly to CdSe–ZnS core–shell QDs. The self-assembly of hexahistidine-appended DNA to QDs is probed with gel electrophoresis and fluorescence resonance energy transfer techniques, and the results confirm high-affinity conjugate formation with control over the average molar ratio of DNA assembled per QD. To demonstrate the potential of this reactive peptide linker strategy, a prototype QD–DNA–dye molecular beacon is self-assembled and tested against both specific and nonspecific target DNAs. This conjugation route is potentially versatile, as altering the reactivity of the peptide linker may allow targeting of different functional groups such as amines and facilitate self-assembly of other nanoparticle–biomolecule structures.

Interest in nanoparticles such as luminescent semiconductor quantum dots (QDs) as well as metallic and magnetic nanocrystals has grown tremendously in the past decade.^{1–6} Biocompatible QDs, in particular, have been developed for use as labels in immunoassays, flow-cytometry, bio-barcoding, DNA arrays, cellular-labeling, and for *in vivo* and deep-tissue imaging.^{1,2,7–12} Luminescent QDs are also attractive for use as donor fluorophores in fluorescence resonance energy transfer- (FRET) based bioassays and as potential sensitizers in photodynamic therapy.^{13,14} They have already been successfully used to assemble FRET-based sensors specific for the detection of nutrients, explosives, proteolysis, enzymes that cleave β -lactam antibiotics, pH sensing, and incorporated into molecular beacons (MB).^{1,15–26} Despite these achievements, further development of QD use

in a broader range of biological assays has largely been hampered by lack of facile methods for creating stable and versatile hybrid QD–biomolecule conjugates.

Presently available QD-bioconjugates are formed using three main approaches, each of which is affected by select problems.^{1,27,28} (1) Cross-linking chemistry, for example, carbodiimide-mediated amide formation or use of bifunctional linkers, targets available functional groups on the QD surface coating and on the biomolecules but necessitates the use of multiple purification steps and may be susceptible to reduced stability and/or aggregation.^{1,28–30} (2) Direct linkage of biomolecules such as thiolated DNA or peptides to the QD surface can be a rapid and relatively simple strategy^{31,32} but necessitates large amounts of bioligands along with cap exchange and purification. (3) Use of biotin–avidin interactions is a more common approach in biology but requires the use of avidin/streptavidin- or biotin-functionalized QDs and often produces large size bioconjugates, which can limit their utility in targeted applications such as FRET analysis and cellular assays.¹ Furthermore, with the above strategies (in particular 1 and 2), it is difficult to achieve control over the number of biomolecules attached to a QD, i.e., bioconjugate valence.

* Corresponding authors. E-mail: imedintz@cbmse.nrl.navy.mil (I.L.M.); bertil.lorenzo@unimo.it (L.B.).

† U.S. Naval Research Laboratory, Center for Bio/Molecular Science and Engineering Code 6900.

‡ S3-INFM-CNR, National Research Center on nanoStructures and bioSystems at Surfaces.

§ U.S. Naval Research Laboratory, Division of Optical Sciences Code 5611.

|| Department of Chemistry and Biochemistry, University of Maryland.

§ Present address: Ecole de Physique et Chimie Industrielle (ESPCI), 10 rue Vauquelin, 75005 Paris, France.

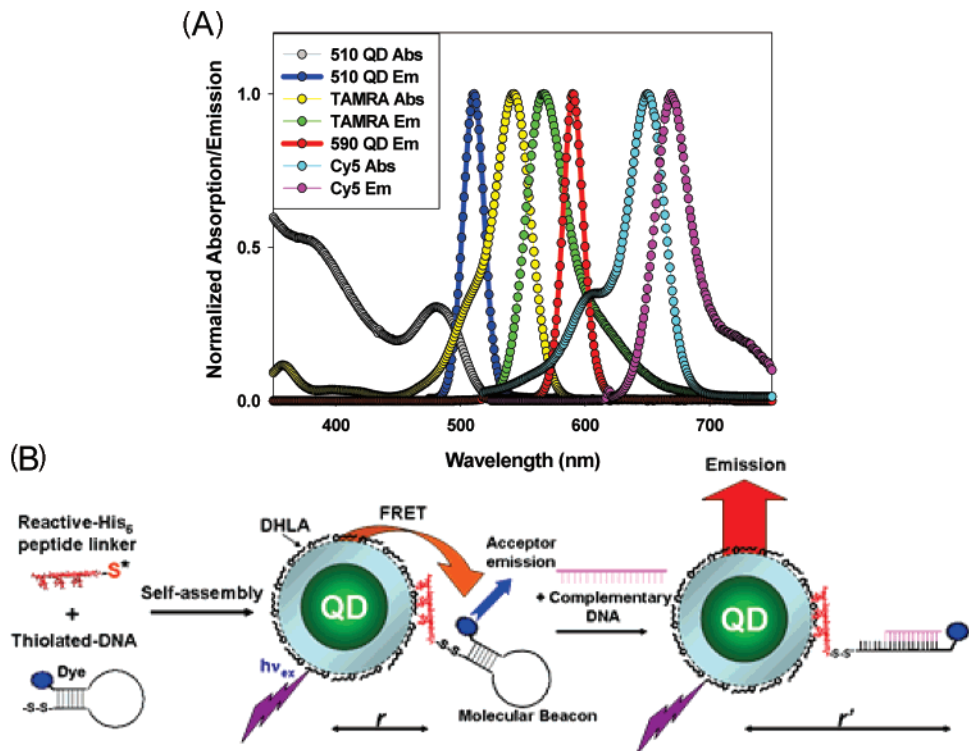


Figure 1. (A) Photophysical properties of QDs and dyes used. Emission spectra of 510 nm (QY \sim 12%) and 590 nm (QY \sim 10%) QDs are plotted along with the 510 nm QD absorption. Absorption/emission spectra of tetramethylrhodamine (TAMRA; $\lambda_{\text{ex}} \sim 540$ nm, $\lambda_{\text{em}} \sim 565$ nm, $\epsilon = 95\,000\, \text{M}^{-1}\, \text{cm}^{-1}$) and Cy5 ($\lambda_{\text{ex}} \sim 650$ nm, $\lambda_{\text{em}} \sim 670$ nm, $\epsilon = 250\,000\, \text{M}^{-1}\, \text{cm}^{-1}$) are also shown. The Förster distance R_0 for the 510 nm QD–TAMRA and 590 nm QD–Cy5 pairs are 42.5 and 49 Å, respectively. (B) Schematic depiction of His₆–peptide-linker facilitated self-assembly of labeled DNA onto QDs (left) and establishment of a hybrid molecular beacon structure (right). The hairpin DNA stem structure brings the dye–acceptor into close proximity r of the QD establishing efficient FRET. Addition of DNA complementary to the molecular beacon unwinds the stem–loop structure altering the donor–acceptor distance to r' and changing FRET efficiency. DHLA–dihydrolipoic acid.

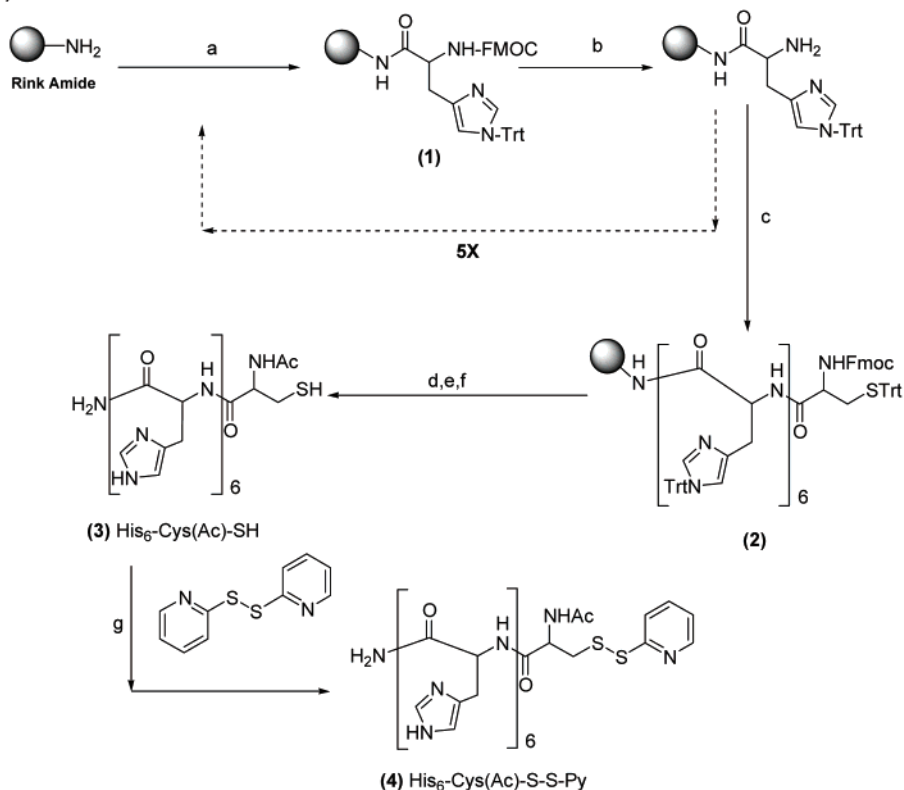
A successful and practical method for creating a variety of QD–bioconjugates should include facile assembly, chemical stability of the final construct, control over the conjugate valence, and the ability to potentially couple emissive QDs to a wide range of biological molecules. Compactness of the final bioconjugates has additional advantages in cellular delivery and the ability to have the QD engage in efficient FRET interactions with proximal dyes if desired. We have developed a conjugation strategy based on metal-affinity-driven interactions between CdSe–ZnS core–shell QDs and proteins or peptides appended with polyhistidine (His_n) tags. This strategy offers some unique advantages such as compactness of the conjugates and the ability to control the number of bioreceptors immobilized on a single QD.³³ We have also recently shown that self-assembly is rapid and has high binding/affinity constants.^{34,35} The use of polyhistidine-driven self-assembly as an alternative strategy for attaching biomolecules to QDs has generated growing interest recently.^{36,37}

In this report, we exploit this strategy and demonstrate the chemical attachment of a reactive hexahistidine (His₆) peptidic linker to DNA oligonucleotides to enable their self-assembly onto QDs. The peptide linker is synthesized to be thiol-reactive, which allows facile attachment to any thiolated-DNA sequence (and an array of other thiolated biomolecules) via disulfide exchange. Synthesis and self-assembly of DNA oligos modified with a peptide linker onto

QDs is characterized with several techniques including gel electrophoresis and FRET. We also demonstrate the potential utility of this His-reactive-peptide modification of DNA by assembling and testing a QD–DNA molecular beacon that specifically detected the presence of its complementary sequence.

Our goal was to develop a bifunctional peptide linker that could allow easy attachment of DNA oligonucleotides at one end while the other is modified with a polyhistidine tag to facilitate self-assembly of the full peptide–DNA complex onto QDs via metal–histidine interactions. The choice of a peptide as the linker was motivated by its ease of synthesis and the wide range of accessible reactive chemistries offered by simply modifying the terminus or other constituent residue. The synthesis of the peptide module was performed by standard solid-phase peptide synthesis (SPPS) on Rink amide resin to create the desired His₆–Cys sequence, see Scheme A of Figure 2 and Supporting Information for specific details on the synthesis.³⁸ A standard acetylation blocking of the terminal amine on the linker was used, as this amine might cause potential problems with subsequent coupling due to its basic, reactive, and complexing nature. Cleavage of the peptide from the resin and concomitant deprotection yielded (**3**) in Scheme A. The crude peptide was precipitated, and the final bifunctional reactive linker His₆–Cys(Ac)–S–S–Py (**4**) was obtained through a direct disulfide exchange reaction. Disulfide exchange was chosen

(A)



(B)

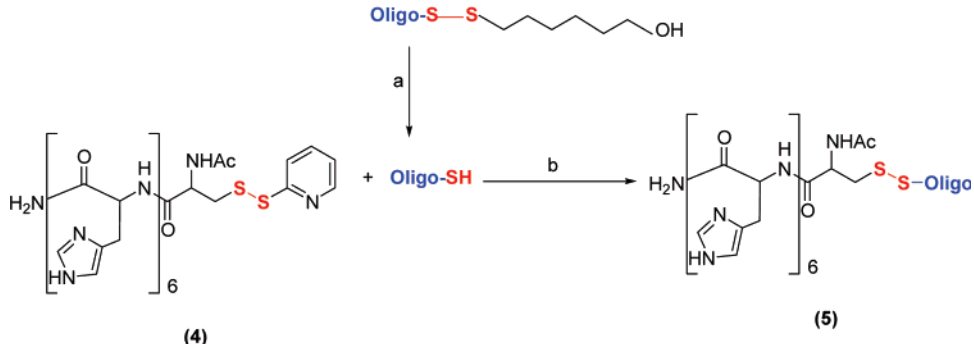


Figure 2. (A) Synthesis, deprotection, and modification of the reactive His₆ peptide linker. See Supporting Information for full chemical names and details of the synthesis. Residue coupling: (a) Fmoc-(Trt)-His-OH 2.5 eq, PyBOP 2.5 eq, DIPEA 5 eq, in DCM for 2 h or (c) Fmoc-(Trt)-Cys-OH 2.5 eq, PyBOP 2.5 eq, DIPEA 5 eq, DCM, overnight. Fmoc deprotection: (b,d) 20% piperidine in DMF, 0.5 h. Terminal amine acylation: (e) acetic anhydride:DCM:DIPEA (1:1:1), 1 h. Cleavage from the resin: (f) TFA:TIS:H₂O (95:2.5:2.5). Modification with pyridyldisulfide: (g) aldrithiol-2, 1 × TAE. (B) Conjugation scheme for generating a His₆-tagged oligopeptide. Reduction of thiol-protected oligo: (a) DTT-KPO₄ buffer pH 8; thiol-exchange: (b) KPO₄-EDTA buffer pH 8.

as the initial reactive chemistry for His₆ attachment to thiolated-DNA because it is one of the fastest and most common linkage chemistries used in bioconjugation; it has also been shown to be both facile and quantitative.^{39,40} Reverse-phase HPLC yielded the reactive bifunctional linker as a pure, stable product.

Functionalization of free 5'-thiol DNA with the peptide linker (4) to yield the His₆-tailed oligo (5) was rapid and straightforward, as outlined in Scheme B of Figure 2. The protected 5'-thiol oligo was first deprotected/reduced with tris(2-carboxyethyl)phosphine hydrochloride (TCEP) or dithiothreitol (DTT) to yield the 5' free thiol and purified (from excess reducing agent) using HPLC or two consecutive PD-

10 gel permeation columns. A slight molar excess (2–3×) of bifunctional reactive linker (4) was then added, and the mixture was allowed to react anywhere from 1 h to overnight. HPLC purification of the 1 h reaction showed that the reaction was quantitative; all the deprotected oligo was peptide modified and the oligopeptide conjugate could be easily recovered (Supporting Information, Figure S1). Purification of His₆-modified DNA from the overnight reaction with a PD-10 column yielded essentially the same result. In our experience, we found the reactive peptide linker could be lyophilized, shipped between Europe and North America, and then stored at –20 °C for over a year, which potentially

Table 1. DNA Sequences Used in This Study^a

| name | sequence | length (bp) | MW | Tm °C |
|---------------------------|---|----------------|--------|----------|
| test oligo 1 | 5'-[ThiSS]-GAGCTCGTTC-[Am-Uni]GTCTGAAGGTGAATGGCAG-3' | 29 | 9419 | 70.3 |
| test oligo 2 | 5'-[ThiSS][TAMdT]-GAGCTCGTCTGAAGGTGAATGGCAG-3' | 30 | 10 385 | 69.9 |
| MB-Cy5 (molecular beacon) | 5'-[ThiSS]- CCGAGCTGGATTAAAGTAT GCTGCTCGG -[AmC3]-3' | 27 | 8665 | 69.2 |
| comp (complement) | 3'-ACCTAATTCTATAACGACGATT-5' | 21 | 6364 | 54.8 |
| noncomp (noncomplement) | 3'-AAAACATGACTATAGCTAGAA-5' | 21 | 6455 | 52.8 |

^a ThiSS: thiol modifier with six-carbon spacer, TAMdT: T modified with (tetramethyl-6-carboxyrhodamine (TAMRA) on six-carbon spacer, AmC3: amino modifier with three-carbon spacer, Am-Uni: amino modifier with five-carbon spacer (see Supporting Information for the structure of the DNA modifications). Stem-forming sequence is in bold. Underlined is loop-forming sequence. Target complementary sequence is in italic.

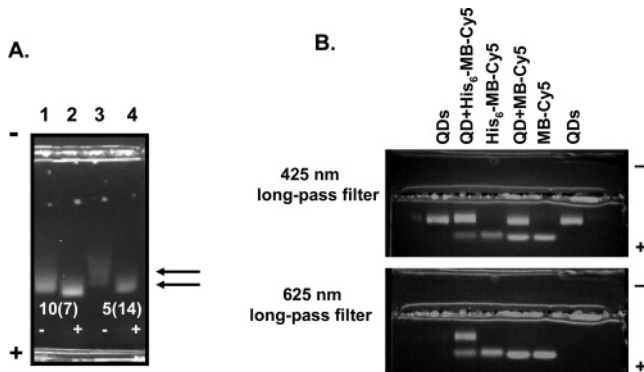


Figure 3. Electrophoretic characterization of QD–DNA self-assembly and absence of thiol interactions with QD surfaces. (A) Agarose gel picture for QDs mixed with oligo: Lanes 1,2: 10 picomoles QDs mixed with DNA to a molar ratio of 7 DNA/QD. Lanes 3,4: 5 picomoles QDs mixed with DNA at 14 DNA/QD. “+” and “-” indicate His-peptide-modified and -unmodified DNA, respectively. (B) Agarose gel pictures for QDs mixed with MB–Cy5; 510 nm QDs were incubated with ~30-fold excess His₆–peptide modified and unmodified MB–Cy5 and imaged using 425 nm long-pass (top) and 625 nm long-pass (bottom) filters. Shown from left to right are QD only controls (lanes 1 and 6), QDs mixed with His₆–MB–Cy5 (lane 2), His₆–MB–Cy5 alone (lane 3), QDs mixed with unmodified MB–Cy5 (lane 4) and MB–Cy5 (lane 5).

allows for large-batch preparation of the peptide linker and subsequent storage until needed.

Our first characterization of the QD–DNA conjugates relied on monitoring changes in the electrophoretic mobility of QDs run on a 2% agarose gel when mixed with His₆-modified and -unmodified DNA (test oligo 1, oligonucleotide sequences are given in Table 1). Our experiments were aimed at proving that the His₆-tag specifically promotes self-assembly onto DHLA-capped QDs. We further wanted to verify that the disulfide group positioned between the linker and oligos is not independently promoting interactions with (and binding to) the QDs. This concern stems from the fact that thiol-terminated peptides and DNA were shown to interact with CdSe–ZnS QDs.^{32,41} In addition, dithiol and sulfide-terminated DNA and molecules are known to effectively interact with gold surfaces and other metal nanoparticles. QD mobility shifts were first monitored as increasing copies of His₆–peptide–DNA were self-assembled onto their surfaces.^{42–45} Figure 3A shows a typical gel image where samples of QD–DNA conjugates at different oligo-to-QD ratios were run side-by-side with control samples of QDs mixed with unmodified oligos. The picture clearly

shows that higher mobility bands are measured for samples containing QDs mixed with (5), the His₆-tailed oligo, (lanes 2 and 4) compared to the lower mobility measured for QDs mixed with unmodified oligo (lanes 1 and 3). The shift of the QD band upon conjugation to the His-modified DNA reflects changes in electrophoretic mobility due to the increased number of negative DNA phosphate charges upon QD–DNA conjugate formation. Control samples with unmodified DNA migrated with lower mobility. Although DHLA-capped QDs are negatively charged in the absence of surface-assembled DNA, they have lower mobility (lanes 1 and 3). This explains partly why only small differences in the mobility shifts were measured for QD–DNA conjugates compared to unconjugated QDs.

To test potential effects of the disulfide (–S–S–) group on binding to QDs, we monitored the electrophoretic mobility shift of DHLA-capped QDs (510 nm emission peak) that were incubated with Cy5-labeled molecular beacon (MB) DNA either unmodified (MB–Cy5) or His-modified (His₆–MB–Cy5). See below for a discussion of the MB DNA structure/function. Both DNA sequences contain the same disulfide bond (see Table 1, Figure 2, and ThiSS structure in Supporting Information Figure S5). Figure 3B shows the gel fluorescence pictures collected using two filter systems: a 425 nm long-pass filter to visualize both QDs and Cy5 emission (top picture), and a 625 nm long-pass filter to visualize Cy5 emission only (bottom picture). These pictures indicate that QDs mixed with unmodified MB–Cy5 show two separate and distinct emission bands for unbound QDs and MB–dye (lanes 4 in both pictures); in addition, the QD band in this sample corresponds to that observed for nanocrystal only samples (lanes 1 and 6, top picture). In comparison, a slightly lower mobility shift band (lane 2) is measured for QDs mixed with His-modified sequences compared to QDs only (lanes 1 and 6), indicating that QD and MB comigrate in the gel and proving conjugate formation. The slower mobility shift (in comparison to what was shown in Figure 3A) may be the result of the bulkier QD–MB conjugates compared to open oligo structures (see discussion below) and the relatively uncharged nature and size of all of the Cy5 dyes attached to the DNA in the QD conjugates. An additional higher mobility (and weaker signal) shift band is observed for the sample of QDs mixed with His₆–MB–Cy5 (lane 2, top picture) identical to the one in lane 3 (His₆–MB–Cy5 alone), resulting from excess unconjugated DNA sequences. Interestingly, His₆ modification

even alters the migration of the MB–Cy5 as evidenced by the small differences in their mobility. The QD–peptide–DNA conjugates were further characterized by atomic force microscopy (AFM) imaging, where association of oligos with a central QD was observed only for samples made of QDs mixed with His₆–peptide–DNA. Additional details and AFM images are provided in the Supporting Information (Figure S2).

These data clearly provide initial evidence that not only does the His₆–peptide linker mediate self-assembly onto the QDs, but that QD–peptide–DNA conjugate integrity, derived from a strong binding affinity, is maintained during migration in a sieving matrix. They also prove that the internal disulfide bonds are “silent” and do not contribute to conjugate formation. We attribute this to several inter-related reasons. First, the disulfide bond in our designed His–peptide linker DNA are drastically different from reduced thiols used to promote thiolated-DNA and peptide attachment to CdSe–ZnS QD surfaces.^{32,41} In contrast to gold, which shows affinity to both reduced (thiol) and oxidized (disulfide) groups alike, QDs selectively interact with single- and multi-thiol ends functions. In fact, we have previously shown that TOP/TOPO-capped CdSe–ZnS QDs effectively cap exchange only with DHLA (with its open dithiol head group), while incubation with thioctic acid (precursor to DHLA) with its closed disulfide ring did not promote cap exchange and water solubility under various treatments (e.g., extending incubation, mild heating, etc.).³⁰ The His-driven binding of the oligos and MBs to the QDs is also not associated with removal of the native DHLA cap. Further, due to their bidentate nature, capping of QDs with either DHLA or DHLA–PEG was found to drastically enhance stability in buffer solutions compared to monothiol-terminated ligands, such as mercaptoacetic and mercaptoundecanoic acids, which are known to have a dynamic on–off rates.^{1,12,30,46} Last, the average number of oligos attached to a QD is too small and would not be able on their own to promote cap-exchange or hydrophilicity of the formed conjugates.

The second characterization tool utilized FRET between the QD and an acceptor dye attached to the His₆-tagged DNA in the conjugate. FRET measurements allowed us to test conjugate formation and to gain insight into the conformation of the His₆–peptide–DNA self-assembled on the nanocrystal surface by providing accurate estimates of the QD–dye donor–acceptor separation distance in these assemblies. For this, tetramethyl-6-carboxyrhodamine- (TAMRA) labeled test oligo 2 was His₆-tail-modified and then self-assembled on 510 nm emitting QDs in the presence of unlabeled test oligo 1 (also His tail-modified). The number of peptide-modified DNAs per QD was maintained at 12 while varying the fraction of labeled to unlabeled copies. This configuration maintains the conjugate QY (Q_D) constant throughout the experiments and provides more accurate information on the His₆–peptide–DNA conformation as it self-assembles on the QD surface, by allowing measurements for the separation distance at several dye-to-QD ratios.^{16,47} Figure 4A shows the PL spectra collected for an increasing number of dye-labeled DNAs per QD. A pronounced loss in QD PL is

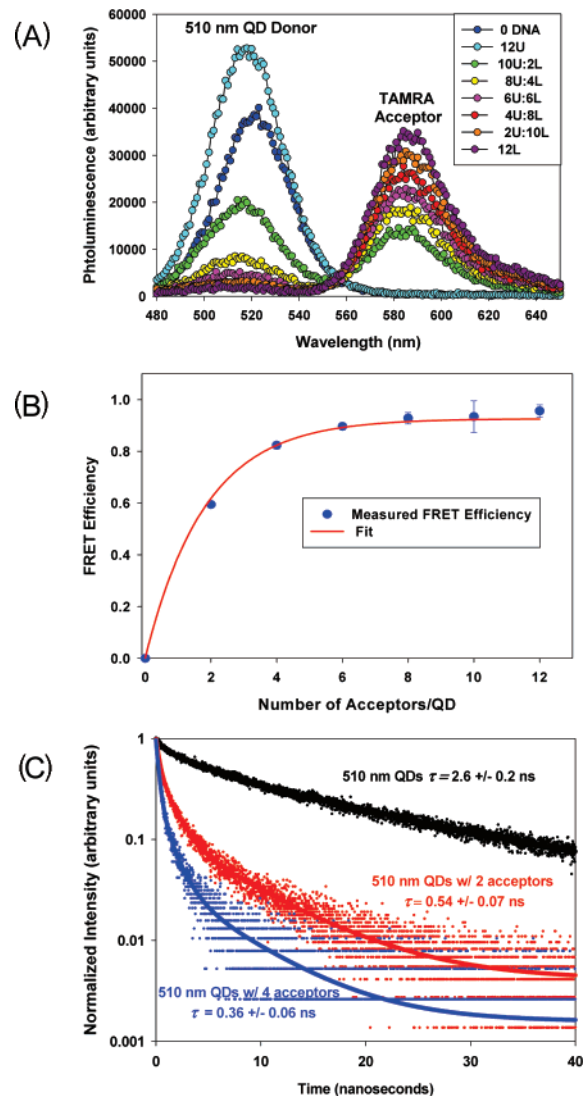


Figure 4. FRET-based characterization of QD–dye-labeled DNA self-assembly. (A) Representative PL spectra from titrating an increasing ratio of peptide-linker-modified TAMRA-labeled test oligo 2 onto 510 nm QDs in the presence of unlabeled test oligo 1. The molar ratio of DNA to QDs was maintained at 12 while varying the ratio of unlabeled to labeled DNA. (B) Plot of FRET efficiency derived from QD donor PL loss as in (A) fitted using eqs 1–3,5 (see Supporting Information). Average of three experiments plus/minus standard deviation. (C) Plot of time-resolved fluorescent emission for 510 nm QD donors self-assembled with 2 and 4 peptide-linker-functionalized TAMRA-labeled DNA.

measured, with 60% quenching efficiency at 2 acceptors per QD and nearly 100% loss at a ratio of 12 dyes per QD. Figure 4B shows the corresponding FRET efficiency derived from the loss in QD PL at each ratio along with a fit using eqs 2 and 5 (Supporting Information). A QD–dye center-to-center separation distance of 40 Å was derived for the QD–oligo-2–TAMRA conjugate. The above experiments also showed that FRET-induced sensitization of TAMRA is initially ~ 2.5 times greater than direct excitation contribution at $n = 2$. However, this steadily decreases with increasing ratio, which may be attributed to inner filtering and/or proximity quenching when multiple TAMRA dyes surround a QD.⁴⁸ Control experiments performed using unmodified TAMRA-labeled

test oligo 2 resulted in lower quenching efficiency, which we attribute to “solution-phase” FRET, as described by a Stern–Volmer analysis (see Supporting Information, Figure S3).

The steady-state fluorescence data were further complemented with time-resolved fluorescence experiments, where changes in the excited-state fluorescent lifetime (τ) of QD PL in the absence and presence of peptide-modified TAMRA-labeled test oligo 2 were measured. Figure 3D shows that a marked loss in the average QD fluorescent lifetime is measured for QDs conjugated to TAMRA-labeled DNA, with $\tau = 2.6$ ns for $n = 0$, $\tau = 0.54$ ns at $n = 2$, and $\tau = 0.36$ ns at $n = 4$, respectively. The corresponding FRET efficiencies derived using the relation ($E = (1 - \tau_n)/\tau_{n=0}$)⁴⁸ are in reasonable agreement with the values reported in Figure 3C. Overall, this confirms resonance energy transfer to proximal TAMRA dyes as the primary source for the QD PL quenching mechanism.

Taking into account that the inorganic core radius of the 510 nm emitting nanocrystals is ~ 25 Å,^{18,49} we derive a lateral spatial extension to the acceptor dye for the His₆–peptide–DNA of ~ 15 Å. Because the His tag drives self-assembly by interacting directly with the metallic surface, its contribution to the measured distance can essentially be neglected.⁵⁰ The lateral extension (~ 15 Å) reflects well the sequence length and conformation (at equilibrium) anticipated for the linker–DNA–TAMRA complex, with a six-carbon ThiSS linker, the modified dT base and the additional six-carbon bridge to the TAMRA dye center (additional details are provided in the Supporting Information, Figure S5).⁵¹ We also believe that electrostatic repulsion between adjacent oligos and between oligos and charged COOH groups present at the end of the DHLA promote a well-extended conformation of the linker-DNAs in the conjugate and prevent them from folding on the nanocrystal surface. His₆-tagged dye-labeled DNA were also self-assembled to QDs surface-functionalized with DHLA modified with PEG of molecular weight 600 (data not shown).^{35,46}

Confident in the ability of the His₆-tagged-reactive peptide to specifically mediate DNA self-assembly onto CdSe–ZnS QDs, as verified by gel mobility and FRET data above, we set out to demonstrate a potential use for such conjugates by assembling a QD–MB (QD–molecular beacon conjugate) and testing its ability to specifically sense its target (see schematic in Figure 1B). Molecular beacons are commonly used to perform genetic analysis due to their essentially reagentless function. They can easily signal the presence or absence of target DNA/RNA sequence(s) in a reaction by monitoring changes in FRET interactions between two fluorophores attached at the ends of the MB sequence.^{52,53} For this, a *bis*-functionalized oligo, thiol-modified at the 5'-end and amino-modified at the 3'-end, was obtained from Operon (see MB–Cy5 sequence in Table 1). Following labeling with Cy5 dye, and modification with the His₆–peptide linker (as detailed in the Supporting Information section), the MB–Cy5 was self-assembled onto DHLA-capped QDs. In nondenaturing conditions, the native oligo is designed to form a stem–loop structure, due to comple-

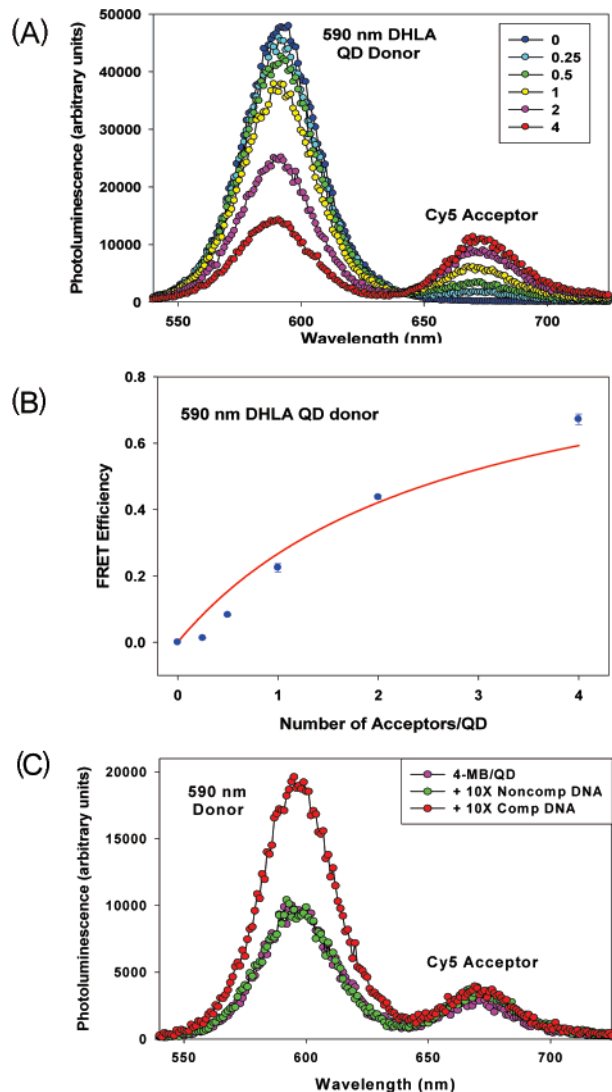


Figure 5. Characterization of Cy5-labeled DNA assembly onto 590 nm DHLA-capped QDs. (A) PL spectra collecting from titrating an increasing ratio of peptide-linker–MB–Cy5 DNA onto QDs. (B) Plot of the FRET efficiencies derived from QD donor PL loss in (A). The lines represent a fit of the FRET efficiency as in Figure 3. (C) Plot of PL emission for 590 nm QD–MB sensors after self-assembly with 4 peptide-functionalized MB–Cy5 DNA and response in the presence of 10-fold molar excess complementary and noncomplementary DNA.

mentarity of the sequences at the 3' and 5' ends, which brings the dye close to the QD and initiates FRET interactions between the two fluorophores and produces QD PL loss.^{52–54} Addition of appropriate complementary target DNA, which hybridizes to the loop, opens the stem structure and results in a systematic change in the FRET efficiency that can be directly correlated with the target concentration.

We first evaluated self-assembly of His₆–peptide-linker–MB–Cy5 onto 590 nm DHLA-capped QDs. Figure 5A shows the fluorescence spectra collected from assembling increasing copies of His₆–peptide-linker–MB–Cy5 onto DHLA-capped 590 nm QDs. Figure 5B shows a plot of the corresponding FRET efficiency (derived from QD PL loss) as a function of the number of MB–Cy5 per QD. A progressive and pronounced rate of FRET was measured with

increasing MB–Cy5-to-QD ratios, similar to the results shown in Figure 2B, with \sim 70% PL loss measured at 4-MB–Cy5 per QD conjugate. The larger scattering in the experimental data (compared to Figure 3C) can be attributed to small heterogeneities (in position and orientation) of the QD–MB–Cy5 self-assembly because there is more than one conformation for each of the beacons on the nanocrystal surface. A fit of the FRET efficiency to the data provided an estimate for the average donor–acceptor separation distance of \sim 58 \pm 4 \AA . Using a radius of \sim 35 \AA for the inorganic core of 590 nm QDs would place the Cy5 dye at \sim 23 \AA away from the nanocrystal surface. This average lateral extension of the molecular beacon is larger than that measured for TAMRA-labeled oligo 2 above, which can be attributed to differences between the structures of the two systems and to the ability of the beacon stems to rotate around the dithiol linkage. The larger distance also accounts for the structure of the Cy5 attachment to the 3' end of the beacon, where an additional multicarbon linker to the terminal amine is involved. To test the ability of the QD–MB to detect the presence of its target, a ratio of 4-MB–Cy5 per QD was chosen for the QD–MB configuration, as it satisfies a few relevant criteria. First, a substantial rate of FRET is measured at this ratio. Second, subsequent change in the FRET efficiency following addition of the target DNA will produce a large change in the PL intensity for easy measurements. Third, at this ratio, all the QDs will have MB–Cy5 assembled on their surfaces, with the distribution centered at \sim 4 per QD.^{33,45} Figure 5C shows changes in the composite PL spectra following addition of a 10 \times concentration of the complementary DNA to a solution of self-assembled QD–MB–Cy5 conjugates; a sizable recovery of the QD PL signal (\sim doubling of the initial signal), corresponding to a reduction of the FRET efficiency from 70% to 35% is measured. In comparison, adding a noncomplementary DNA had no discernible effect on the fluorescence spectra. These changes indicate that, on average, the Cy5 has moved away from the QD surface following unwinding of the stem–loop structure. The DNA section of the MB–Cy5 at equilibrium now consists of both single- (closed-loop, high FRET efficiency) and double-stranded DNA (low FRET efficiency) and can assume several configuration formations with freedom of three-dimensional movement relative to the QD surface. This complexity allows only an approximate estimate of the range of possible changes in the QD–dye separation distance, from \sim 12–13 \AA (using Supporting eq 1 and assuming a homogeneous conformation within the QD–DNA population), to a maximum 60 \AA change for a fully extended double-stranded DNA compared to its original position in the stem loop structure.

We note that the FRET-induced Cy5 emission measured at a 1:1 QD:MB–Cy5 ratio was markedly larger than that due to the direct excitation contribution (\sim 40 times larger, see Supporting Information Figure S4). This contrasts with the smaller difference observed for the 510 nm QD–TAMRA pair above, a result that reflects where the systems are excited relative to their absorptions and the differences in the photophysical properties between the two dye fami-

lies: rhodamine vs cyanine. In addition, changes in QD PL (recovery) upon addition of the target sequence was accompanied by negligible change in Cy5 PL, which may again reflect interactions of the dye with the solution environment in the open stem sequence, a result similar to what was reported for other QD DNA–Cy5 conjugates.⁵⁵ Finally, we would like to emphasize that iterative optimization of the DNA structure, and use of a different QD–dye pair can allow a broad range of FRET responses to be accessed. Furthermore, the improved FRET efficiency, resulting from the unique configuration of having a single donor interact with multiple acceptors,^{1,49} can permit the use of longer DNA sequences within these supramolecular assemblies without reducing the accuracy of the collected data.

In this report, we have illustrated the synthesis of a novel thiol-reactive His_6 peptidic linker that could easily be attached to thiol-modified DNA. The resulting peptide–oligo conjugate was used to mediate the controlled self-assembly of DNA onto CdSe–ZnS QDs. Although peptide–DNA conjugates have been synthesized previously, they were almost exclusively used for *in vivo* cellular delivery of oligonucleotides.^{40,56} Our present effort represents a novel and unique use of such materials. Our design criteria focused on imparting two modular functions to the reactive peptide linker in order to simplify both the assembling chemistry and purification procedures. The first modular function focused on the self-assembly to QDs by using the His_n motif. The initial peptide sequence can be synthesized in-house using either standard SPPS, as demonstrated here, or obtained commercially, and the subsequent modification with a pyridyldisulfide to complete the current version of the linker is straightforward. We should emphasize that the linker design is not constrained to the poly-His motif, as combinatorially evolved peptide sequences that bind to a variety of other semiconductors and metals can be readily substituted.⁵⁷ Additionally, a spacer or solubilizing PEGylated functionality can also be incorporated into the peptidyl portion through SPPS or postsynthetic modification as desired. The second modular function focuses on conjugation of the peptide to a variety of biomolecules beyond the particular chemistry demonstrated here. Switching targeting specificity from thiols to other groups can be easily accomplished by introduction of other chemical functionalities. For example, succinimidyl esters or isothiocyanates could be introduced into the reactive linker for targeting primary amines,⁵⁸ which are also readily synthesized into specific sites on DNA or found in random abundance on proteins/peptides. Indeed, potential intracellular applications of these QD–MB hybrids may actually necessitate this switch, as disulfide bridges are susceptible to cleavage by the strongly reducing environment of the cytoplasm.⁵⁶

The potential of this reactive linker was demonstrated by self-assembling several QD–DNA conjugates as well as a QD–MB construct able to discriminate between different sequences of DNA. A variety of other applications, such as highly luminescent multilabeled hybridization probes, are possible using this construct. Preforming MB sensors with different color QDs and then mixing them may allow

“multiplexing”.⁵⁹ Beyond nanoparticle–MBs, this self-assembly technique may be applicable to attaching biomolecules to a variety of other similarly prepared surfaces.

Acknowledgment. I.L.M. and L.B. contributed equally. We acknowledge NRL, L. Chrisey at the Office of Naval Research (ONR grant no. N001404WX20270), Stephen Lee and Ilya Elashvilli of the CB Directorate/Physical S&T Division, DTRA for support. The fluorescent lifetime instrumentation for this work was provided by an NSF-CRIF award (CHE-0342973) to D.S.E.

Supporting Information Available: Details on the synthesis of the thiol-reactive linker, peptide–DNA conjugation, QD synthesis, self-assembly of modified DNA onto QDs, and characterization, analysis of energy transfer data, and supporting results. This material is available free of charge via the Internet at <http://pubs.acs.org>.

References

- Medintz, I.; Uyeda, H.; Goldman, E.; Mattoussi, H. *Nat. Mater.* **2005**, *4*, 435–446.
- Michalet, X.; Pinaud, F. F.; Bentolila, L. A.; Tsay, J. M.; Doose, S.; Li, J. J.; Sundaresan, G.; Wu, A. M.; Gambhir, S. S.; Weiss, S. *Science* **2005**, *307*, 538.
- Daniel, M. C.; Astruc, D. *Chem. Rev.* **2004**, *104*, 293.
- Katz, E.; Willner, I. *Angew. Chem., Int. Ed.* **2004**, *43*, 6042.
- Burda, C.; Chen, X. B.; Narayanan, R.; El-Sayed, M. A. *Chem. Rev.* **2005**, *105*, 1025.
- Nanobiotechnology II*; Niemeyer, C. M., Mirkin, C. A., Eds.; Wiley & Sons: Hoboken, NJ, 2007.
- Goldman, E. R.; Medintz, I. L.; Mattoussi, H. *Anal. Bioanal. Chem.* **2006**, *384*, 560.
- Jaiswal, J. K.; Mattoussi, H.; Mauro, J. M.; Simon, S. M. *Nat. Biotechnol.* **2003**, *21*, 47.
- Gao, X.; Cui, Y.; Levenson, R. M.; Chung, L. W. K.; Nie, S. *Nat. Biotechnol.* **2004**, *22*, 969.
- Kim, S.; Lim, Y. T.; Soltesz, E. G.; De Grand, A. M.; Lee, J.; Nakayama, A.; Parker, J. A.; Mihaljevic, T.; Laurence, R. G.; Dor, D. M.; Cohn, L. H.; Bawendi, M. G.; Frangioni, J. V. *Nat. Biotechnol.* **2004**, *22*, 93.
- Chattopadhyay, P. K.; Price, D. A.; Harper, T. F.; Betts, M. R.; Yu, J.; Gostick, E.; Perfetto, S. P.; Goepfert, P.; Koup, R. A.; De Rosa, S. C.; Bruchez, M. P.; Roederer, M. *Nat. Med.* **2006**, *12*, 972.
- Alivisatos, A. P.; Gu, W.; Larabell, C. A. *Annu. Rev. Biomed. Eng.* **2005**, *7*, 55.
- Clapp, A. R.; Medintz, I. L.; Mattoussi, H. *ChemPhysChem* **2005**, *7*, 47.
- Bakalova, R.; Ohba, H.; Zhelev, Z.; Ishikawa, M.; Baba, Y. *Nat. Biotechnol.* **2004**, *22*, 1360.
- Medintz, I. L.; Clapp, A. R.; Melinger, J. S.; Deschamps, J. R.; Mattoussi, H. *Adv. Mater.* **2005**, *17*, 2450.
- Medintz, I. L.; Clapp, A. R.; Mattoussi, H.; Goldman, E. R.; Fisher, B.; Mauro, J. M. *Nat. Mater.* **2003**, *2*, 630.
- Goldman, E.; Medintz, I.; Whitley, J.; Hayhurst, A.; Clapp, A.; Uyeda, H.; Deschamps, J.; Lassman, M.; Mattoussi, H. *J. Am. Chem. Soc.* **2005**, *127*, 6744.
- Medintz, I. L.; Clapp, A. R.; Brunel, F. M.; Tiefenbrunn, T.; Uyeda, H. T.; Chang, E. L.; Deschamps, J. R.; Dawson, P. E.; Mattoussi, H. *Nat. Mater.* **2006**, *5*, 581.
- Shi, L. F.; De Paoli, V.; Rosenzweig, N.; Rosenzweig, Z. *J. Am. Chem. Soc.* **2006**, *128*, 10378.
- Levy, M.; Cater, S. F.; Ellington, A. D. *ChemBioChem* **2005**, *6*, 1.
- Tomasulo, M.; Yildiz, I.; Raymo, F. M. *J. Phys. Chem. B* **2006**, *110*, 3853.
- Xu, C. J.; Xing, B. G.; Rao, H. H. *Biochem. Biophys. Res. Commun.* **2006**, *344*, 931.
- Zhang, C. Y.; Yeh, H. C.; Kuroki, M. T.; Wang, T. H. *Nat. Mater.* **2005**, *4*, 826.
- Zhang, C. Y.; Johnson, L. W. *J. Am. Chem. Soc.* **2006**, *128*, 5324.
- Snee, P. T.; Somers, R. C.; Nair, G.; Zimmer, J. P.; Bawendi, M. G.; Nocera, D. G. *J. Am. Chem. Soc.* **2006**, *128*, 13320.
- Cady, C. N.; Strickland, A. D.; Batt, C. A. *Mol. Cell. Probes* **2007**, *21*, 116.
- Klostranec, J. M.; Chan, W. C. W. *Adv. Mater.* **2006**, *18*, 1953.
- Pons, T.; Clapp, A. R.; Medintz, I. L.; Mattoussi, H. Luminescent Semiconductor Quantum Dots in Biology. In *Nanobiotechnology II*; Niemeyer, C. M., Mirkin, C. A., Eds.; Wiley & Sons: Hoboken, NJ, 2007; p 141.
- Dubertret, B.; Skourides, P.; Norris, D. J.; Noireaux, V.; Brivanlou, A. H.; Libchaber, A. *Science* **2002**, *298*, 1759.
- Matoussi, H.; Mauro, J. M.; Goldman, E. R.; Anderson, G. P.; Sundar, V. C.; Mikulec, F. V.; Bawendi, M. G. *J. Am. Chem. Soc.* **2000**, *122*, 12142.
- Gill, R.; Willner, I.; Shweky, I.; Banin, U. *J. Phys. Chem. B* **2005**, *109*, 23715.
- Pinaud, F.; King, D.; Moore, H.-P.; Weiss, S. *J. Am. Chem. Soc.* **2004**, *126*, 6115.
- Pons, T.; Medintz, I. L.; Wang, X.; English, D. S.; Mattoussi, H. *J. Am. Chem. Soc.* **2006**, *128*, 15324.
- Hainfeld, J. F.; Liu, W.; Halsey, C. M. R.; Freimuth, P.; Powell, R. D. *J. Struct. Biol.* **1999**, *127*, 185.
- Sapsford, K. E.; Pons, T.; Medintz, I. L.; Higashiya, S.; Brunel, F. M.; Dawson, P. E.; Mattoussi, H. *J. Phys. Chem. C* **2007**, in press.
- Zhou, M.; Ghosh, I. *Biopolymers* **2007**, *88*, 325.
- Ipe, B. I.; Niemeyer, C. M. *Angew. Chem., Int. Ed.* **2006**, *45*, 504.
- Amblard, M.; Fehrentz, J. A.; Martinez, J.; Subra, G. *Mol. Biotechnol.* **2006**, *33*, 239.
- Berti, L.; Xie, J.; Medintz, I. L.; Glazer, A. N.; Mathies, R. A. *Anal. Biochem.* **2001**, *292*, 188.
- Venkatesan, N.; Kim, B. H. *Chem. Rev.* **2006**, *106*, 3712.
- Mitchell, G. P.; Mirkin, C. A.; Letsinger, R. L. *J. Am. Chem. Soc.* **1999**, *121*, 8122.
- Parak, W. J.; Gerion, D.; Zanchet, D.; Woerz, A. S.; Pellegrino, T.; Michelet, C.; Williams, S. C.; Seitz, M.; Bruehl, R. E.; Bryant, Z.; Bustamante, C.; Bertozzi, C. R.; Alivisatos, A. P. *Chem. Mater.* **2002**, *14*, 2113.
- Chan, P. M.; Yuen, T.; Ruf, F.; Gonzalez-Maeso, J.; Sealfon, S. C. *Nucleic Acids Res.* **2005**, *33*.
- Gerion, D.; Pinaud, F.; Williams, S. C.; Parak, W. J.; Zanchet, D.; Weiss, S.; Alivisatos, A. P. *J. Phys. Chem. B* **2001**, *105*, 8861.
- Pons, T.; Uyeda, H. T.; Medintz, I. L.; Mattoussi, H. *J. Phys. Chem. B* **2006**, *110*, 20308.
- Uyeda, H. T.; Medintz, I. L.; Jaiswal, J. K.; Simon, S. M.; Mattoussi, H. *J. Am. Chem. Soc.* **2005**, *127*, 3870.
- Sapsford, K. E.; Pons, T.; Medintz, I. L.; Mattoussi, H. *Sensors* **2006**, *6*, 925.
- Lakowicz, J. R. *Principles of Fluorescence Spectroscopy*, 3rd ed.; Springer: New York, 2006.
- Clapp, A. R.; Medintz, I. L.; Mauro, J. M.; Fisher, B. R.; Bawendi, M. G.; Mattoussi, H. *J. Am. Chem. Soc.* **2004**, *126*, 301.
- Medintz, I. L.; Konnert, J. H.; Clapp, A. R.; Stanish, I.; Twigg, M. E.; Mattoussi, H.; Mauro, J. M.; Deschamps, J. R. *Proc. Natl. Acad. Sci. U.S.A.* **2004**, *101*, 9612.
- Watson, J. D.; Baker, T. A.; Bell, S. P.; Gann, A.; Levine, M.; Losick, R. *Molecular Biology of the Gene*, 5th ed.; Benjamin Cummings Publishing: Reading, MA, 2004.
- Broude, N. E. *Trends Biotechnol.* **2002**, *20*, 249.
- Kwok, P. Y. *Annu. Rev. Genomics Hum. Genet.* **2001**, *2*, 235.
- Tyagi, S.; Kramer, F. R. *Nat. Biotechnol.* **1996**, *14*, 303.
- Zhang, C. Y.; Johnson, L. W. *Anal. Chem.* **2006**, *78*, 5532.
- Nitin, N.; Santangelo, P. J.; Kim, G.; Nie, S. M.; Bao, G. *Nucleic Acids Res.* **2004**, *32*.
- Sarikaya, M.; Tamerler, C.; Schwartz, D. T.; Baneyx, F. O. *Annu. Rev. Mater. Res.* **2004**, *34*, 373.
- Bioconjugate Techniques*; Hermanson, G. T., Ed.; Academic Press: San Diego, CA, 1996.
- Clapp, A. R.; Medintz, I. L.; Uyeda, H. T.; Fisher, B. R.; Goldman, E. R.; Bawendi, M. G.; Mattoussi, H. *J. Am. Chem. Soc.* **2005**, *127*, 18212.

NL070782V